Charge transfer in ion-molecule collisions at keV energy regime: Study of $H^+ + H_2$ collisions by the electron-translation-factor—modified molecular-orbital—expansion method

M. Kimura
Joint Institute for Laboratory Astrophysics, University of Colorado and National Bureau of Standards, Boulder, Colorado 80309
(Received 25 January 1985)

Charge transfer in $H^+ + H_2(X^1\Sigma_g; v=0)$ collisions has been studied theoretically at energies from 0.2 to 20 keV with use of a molecular-state—expansion method incorporating electron translation factors. Two-state semiclassical close-coupling calculations have been performed to investigate the ion-molecule collision dynamics. The molecular states, used as the expansion basis, have been obtained by using the diatoms-in-molecules (DIM) method as functions of the internuclear distance R and two molecular orientation angles θ and ϕ. The effect of orientation of the target molecule on the charge-transfer mechanism has been examined and the charge-transfer cross section is found to be very sensitive to the molecular orientation at energies below 0.5 keV or above 10 keV. Between these energies, however, the orientation effect was small (due to accidental near-degeneracy of the probability from different θ). Our results are in good agreement with experimental measurements in the energy range where they are available.

I. INTRODUCTION

Charge transfer in ion-atom collisions has been a subject of extensive study, theoretically and experimentally. In low- to intermediate-energy regions, eigenfunction-expansion methods based either on a molecular representation or an atomic representation usually have been considered appropriate for applications. However, due to the neglect of so-called electron-translation factors (ETF's) in the molecular-orbital expansion, a fundamental difficulty has been encountered; namely, the scattering wave function is not Galilean invariant. Only recently has the molecular-orbital (MO) method, incorporating the ETF's, been applied to study collision dynamics in one-electron systems.[1-5] On the other hand, while there exists no fundamental difficulty in the treatment of the ETF's in the atomic-orbital (AO) method, it has been recognized that a simple two-center AO—expansion method is defective particularly when a close collision is important.

To describe the molecular character properly at small internuclear separations,[2] united-atom orbitals as well as the two-center AO's are included in the modified AO—expansion method. This pseudostate AO method (or AO+ method) has been applied to the various one-electron systems with much success.[7,8] In the intermediate-energy regime, it has been shown that use of the ETF-modified MO method and AO+ method produce almost identical results in most one-electron systems.[8]

Turning to ion-molecule collisions, there is a surprising lack (virtually none) of rigorous theoretical investigations on dynamics which occur in ion-molecule collisions in the low- to intermediate-energy regime. The reason is twofold: (i) it is quite a complex problem to obtain reasonably accurate adiabatic potentials and eigenfunctions as functions of internuclear coordinates and molecular orientations for the polyatomic system; (ii) for the polyatomic system, the number of internal degrees of freedom that need a proper dynamical treatment increases dramatically.

These aspects of ion-molecule systems have created the nearly impenetrable barriers for theoretical atomic physicists. Some attempts have been made[9,10] to study charge transfer in ion-molecule collisions in the keV energy region by applying the AO—expansion method. Unfortunately, these attempts employed a drastic approximation in the evaluation of matrix elements appearing in the coupled equation; hence, the results are either in poor accord with measurements[9] or only in qualitative agreement.[10] Furthermore, as we have stated earlier, if the small impact parameters are important in the collision, then the simple AO—expansion method is not valid in the low-to intermediate-energy region.

At high energies ($E > 50$ keV), the perturbation method has been used by Tuan and Gerjuoy,[11] and by Band[12] to study charge transfer in $H^+ + H_2$ collisions. Having utilized the method based on the Born approximation, they have calculated total charge-transfer cross sections and also the ratio of the cross sections for process $H^+ + H \rightarrow H^+ + H$ and $H^+ + H_2 \rightarrow H + H_2^+$, $\sigma(H)/\sigma(H_2)$ as functions of the incident energy. The conclusions drawn by these two groups are entirely different and the discrepancy has remained unresolved particularly for energies below 25 keV.

Below ~ 10 eV, however, where rearrangement collisions of heavy particles (chemical reaction) becomes an important process, the investigation of the chemical reaction process is one of the most active fields in theoretical chemistry. In particular, reliable information on energy surfaces for various polyatomic systems as well as reliable methods for determining the surfaces have become available recently. Of these methods, the diatoms-in-molecules[13] (DIM) method possesses several attractive features for application to the scattering problem.[14] This approach, based on the valence-bond (VB) method, parti-

tions the Hamiltonian into diatomic and atomic fragments. Thus all reliable theoretical, as well as experimental, data for the energies of the diatomic molecules and the atoms are used to represent the fragments. The accuracy of this method for some triatomic cases has been tested with regard to the equilibrium distance, the dissociation energies, and other molecular quantities. In some cases it has been found that this method can provide better results than the simple self-consistent-field—configuration interaction (SCF-CI) method.

In this work, we have applied the DIM method to the $H^+ + H_2$ system to obtain reasonably accurate molecular wave functions and corresponding eigenenergies; and we have derived the coupled equations within the semiclassical formalism. We have also given a theoretical rationale for the earlier *ad hoc* treatment[15] of nonadiabatic coupling, showing that this method is indeed equivalent to the inclusion of electron-translation factors (ETF's) in the scattering wave function. We have also studied the effect of molecular orientation on the charge-transfer mechanism.

Since the keV energy region is of interest here, the collision time is far shorter than the vibrational and the rotational periods of the molecule. This fact allows us to assume that vibrational and rotational motions of the target molecule can be frozen during the collision (sudden adiabatic approximation). Hence, the Franck-Condon approximation should be appropriate to describe the nuclear motion during the transition in the molecule.

II. MOLECULAR STATES (DIM METHOD)

The DIM method, first proposed by Ellison,[13] has been extensively developed by Tully and others[14–16] in conjunction with the study of the dynamics of chemical reactions. The DIM method has already proved itself as a powerful tool for investigating the electronic structure of polyatomic molecules in large measure due to its simplicity, although its range of applicability and accuracy are still being tested. We briefly outline the method here.

Consider a polyatomic system with N atoms $a,b,c,\ldots$ containing $n_a, n_b \ldots$ electrons in each atom within the Born-Oppenheimer approximation. Assuming normalized and antisymmetrized atomic orbitals $\xi_M^{(\alpha)}$ are defined for each atom M with α indicating all quantum numbers, we construct a set of n-electron product functions ϕ_m:

$$\phi_m = \prod_M \xi_M^{(\alpha_M)} , \tag{1}$$

where m denotes all of the indices of each atom, i.e., $m=\{\alpha,\beta\ldots\}$. Then, using the functions of Eq. (1), the polyatomic basis functions (PBF's) ϕ_m, which are the bases for the DIM method, are given by

$$\Phi_M = \mathcal{A}\phi_m , \tag{2}$$

where $\mathcal{A}$ is the n-electron antisymmetrizer.

The Kth molecular eigenfunction Ψ_K then can be written as a linear combination of the PBF's.

$$\Psi_K = \sum_M C_{KM}\Phi_M . \tag{3}$$

Equation (3) leads us to the usual eigenvalue equations with the eigenvalue E_K. It is written in the matrix form

$$\underline{H}\underline{C} = \underline{S}\underline{C}\underline{E} , \tag{4}$$

where $\underline{H}$ and $\underline{S}$ represent the Hamiltonian matrix and the overlap matrix, respectively, and both are Hermitian.

Next, following Ellison,[13] we partition the Hamiltonian into the diatomic and the atomic fragments, as can be shown in the matrix form,

$$\underline{H} = \sum_{L=1}^{N} \sum_{\substack{M=1 \\ M>L}}^{N} \underline{H}^{(LM)} - (N-2) \sum_{L=1}^{N} \underline{H}^{(L)} . \tag{5}$$

In Eq. (5), $\underline{H}^{(LM)}$ and $\underline{H}^{(L)}$ are fragment Hamiltonian matrices for an isolated diatomic fragment LM and for an isolated atom L, respectively. Formally, Eq. (5) is *exact.* However, the fundamental approximation in the DIM method is to construct each Hamiltonian matrix by involving only those electrons assigned to each fragment: This enables us to determine these partitioned diatomic as well as atomic fragment matrix elements purely from experimentally and/or theoretically known information about atoms and diatomic molecules. Because of this approximation, the DIM method may not be able to obtain accurate potential curves in the small-R region, say, $R \leq 1$ a.u. where electron correlations among fragments become important. Once this information is available for a range of values of the internuclear coordinate of the diatomic molecule, then the problem reduces to the conventional eigenvalue problem. We have used the zero-overlap (ZO) approximation to solve Eq. (4), in which case the matrix $\underline{S}$ in Eq. (4) is taken to be the unit matrix. Extensive work[13–16] on the treatment of the matrix $\underline{S}$ has revealed that the ZO approximation and explicit inclusion of the matrix $\underline{S}$ obtained from using a simple valence-bond type approximation for the PBF's of Eq. (2) give very similar results to the roots of Eq. (4). This indicates that an accurate treatment of the matrix $\underline{S}$ is probably not necessary.

For the present H_3^+ system, the DIM method requires us to diagonalize a 3×3 matrix element constructed from the diatomic fragment Hamiltonian matrices, involving $H_2(X^1\Sigma_g)$, $H_2^+(1s\sigma_g)$, and $H_2^+(2p\sigma_u)$ states and the atomic fragment Hamiltonian matrix of the $H(1s)$ state in Eq. (5). This yields three roots corresponding to $[H^+ + H_2(X^1\Sigma_g)]$, $[H(1s) + H_2^+(1s\sigma_g)]$, and $[H(1s) + H_2^+(2p\sigma_u)]$ states asymptotically. We have used the Kolos and Wolniewicz[17] theoretical results for H_2 molecular eigenvalues, obtained from a large-scale James and Coolidge-type calculation, and the Bates and Carson[18] method for H_2^+ molecular ion eigenvalues, which solves the nonrelativistic adiabatic eigenvalue problem "exactly."

As we discussed earlier, since the relative collision velocity is so high compared to that associated with the vibrational and rotational motions of the H_2 molecule, the sudden adiabatic approximation for the molecular nuclear motion should be an appropriate approximation. In fact, we have fixed the internuclear distance of the H_2 molecule at its equilibrium distance, i.e., $R_e = 1.401$ a.u. Figure 1 defines coordinates necessary to describe the projectile H^+ ion (A) and target H_2 (BC) molecule. The figure shows the space-fixed molecular frame, which represents the

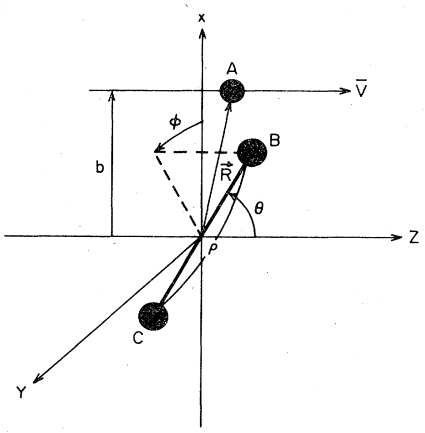

FIG. 1. Coordinate in the laboratory frame for the $H^+ + H_2$ system.

molecule lying with the fixed orientation in the space-fixed frame. We have computed the potential surfaces and wave functions for this case, varying the molecular orientation.

III. COUPLED EQUATIONS

Within the semiclassical formalism, the scattering wave function is expanded in terms of the DIM molecular wave function Φ_i^{DIM} as

$$\Psi = \sum_i a_i(t)\Phi_i^{\mathrm{DIM}}(\mathbf{r};R;\rho)F_i X_i^v(\rho) , \tag{6}$$

where F_i represents the electron-translation factors (ETF's) and X_i^v denotes the vibrational wave function of the molecule. The inclusion of the ETF's is essential to ensure that the scattering wave function satisfies the correct boundary condition. The coupled equations derived for the expansion coefficients a_i have a form similar to that obtained for ion-atom collisions.[3] Within the Franck-Condon approximation, the coupled equations, to first order in $\mathbf{V}$, can be written

$$i\dot{a}_i = \epsilon_i a_i + \sum_j \mathbf{V}\cdot(\mathbf{P}+\mathbf{A})_{ij} M_{ij} a_j , \tag{7}$$

where ϵ_i is the ith state adiabatic potential energy obtained by the DIM method and M_{ij} represents the vibrational overlap matrix, i.e., $M_{ij} = \langle X_i^{v'} | X_j^v \rangle$. $\mathbf{P}$ and $\mathbf{A}$ denote the nonadiabatic coupling and its ETF correction term, respectively. Specifically, these terms have the forms

$$\mathbf{P}_{ij} = \langle \Phi_j^{\mathrm{DIM}} | -i\nabla_R | \Phi_i^{\mathrm{DIM}} \rangle , \tag{8a}$$

$$\mathbf{A}_{ij} = \langle \Phi_j^{\mathrm{DIM}} | [H_{el}, \mathbf{S}_i] | \Phi_i^{\mathrm{DIM}} \rangle , \tag{8b}$$

and

$$\mathbf{S}_i = \tfrac{1}{2} f_i \mathbf{r} , \tag{8c}$$

where f_i represents a so-called switching function which is defined only at the asymptotic region as $f_i \to \pm 1$ (on A or B site). Detailed discussion of this switching function can be found in Ref. 19. The coupling $\mathbf{P}$ and $\mathbf{A}$ can be divided into two contributions in the rotating-frame coordinate, namely, the radial coupling and the angular coupling. The coupled equations (7) can be easily solved numerically, and the corresponding scattering amplitude a_i can be obtained at all times t.

In the present application to $H^+ + H_2$ collisions, only two channels are considered for inclusion in the coupled equations, namely, the initial channel which corresponds to $H^+ + H_2(X^1\Sigma_g: v=0)$ and the final channel corresponding to $H(1s) + H_2^+(1s\sigma_g: v=v')$. These channels are connected through the radial coupling matrix elements given in Eq. (8).

Assuming the $f_i = \pm 1$ depending upon the site of the electron for all values of R (this procedure is equivalent to the application of the first-order atomic ETF on the Born-Oppenheimer wave function), we can show that the "correct" radial coupling matrix element, $(\mathbf{P}+\mathbf{A})^R$ with the DIM wave function of Eq. (3) is

$$(\mathbf{P}+\mathbf{A})_{ij}^R = \sum_M \sum_N C_{iM} \frac{d}{dR} C_{jN} . \tag{9}$$

The nonadiabatic coupling matrix $\mathbf{P}$ contains not only the "real" coupling arising from the change of character of the electronic wave functions as they adjust to the moving molecular field, but also the "fictitious" coupling arising from simple translation of atomic states with the moving nuclei. The ETF correction term $\mathbf{A}$ identifies and cancels the fictitious part of $\mathbf{P}$ that only represents displacement of basis functions with the moving nuclei. Therefore, $(\mathbf{P}+\mathbf{A})$ represents the real coupling. Without inclusion of the ETF correction term, the nonadiabatic coupling shows origin-dependence of the electron coordinate. Hence, the cross section cannot be determined uniquely. In an earlier treatment,[14,15] the fictitious part of the coupling was ignored in the calculation by assuming *a priori* that the contribution from this term should be small in the low-energy collision. However, as we have proved above, this fictitious coupling term is exactly canceled out by the inclusion of the ETF, so that the previous treatment is "accidentally" correct.

The required vibrational overlap matrix elements were computed numerically from the accurate $H_2(X^1\Sigma_g, v)$ and $H_2^+(1s\sigma_g, v')$ potential energies for $v'=0$–20. However, the partial charge-transfer cross section forming the $H_2^+(v')$ ion with $v' \geq 11$ contributes less than 1% to the total charge-transfer cross section. Therefore, most of the calculations shown below have been performed by including the final vibrational state up to $v'=10$.

IV. RESULTS AND DISCUSSION

The dependence of the calculated results on the collision energy and on the molecular orientation is presented in this section. In the calculation the projectile is always on the x-z plane, while the target molecule changes its orientation with respect to θ and ϕ. As we will show later, the θ dependence of the molecular orientation is found to be substantially stronger than its ϕ dependence, and hence, our example chosen for discussion is mainly for the θ orientation.

TABLE I. Comparison of potential parameters R_e and D_e for linear and equilateral configuration of H_3^+.

	DIM (Ref. 15)	*ab initio* (Ref. 20)	DIM (Present)
	Linear configuration		
R_e (a.u.)	1.53	1.54	1.54
D_e (a.u.)	−1.299	−1.280	−1.288
	Equilateral configuration		
R_e (a.u.)	1.498	1.429	1.478
D_e (a.u.)	−1.356	−1.348	−1.352

A. Adiabatic potentials

The adiabatic potential surfaces for the H_3^+ system have been studied extensively by both *ab initio* and semiempirical methods, including the DIM method.[15] A comparison of the equilibrium distance R_e, and the dissociation energy D_e, is shown in Table I. First, we should note that the differences between the present results and those of Preston and Tully,[15] who used the same DIM method, might be due to their fitting of the diatomic data with the Morse potential (in the present work we use a purely numerical method). The better apparent agreement of our potential with the *ab initio* calculation by Conroy[20] may be due to this as well.

The calculated adiabatic potential curves are shown in Fig. 2 for several values of θ with $\phi=0°$. It might be worthwhile to note that for the ground state ($H^+ + H_2$), although molecular orientation effects are apparent for $R \lesssim 2$ a.u., the potential curves are essentially identical for $R > 2$ a.u., independent of the molecular orientation. The figure indicates that the colliding particle can approach more closely at $\theta=90°$ than at $\theta=0°$, since they do not experience strong nuclear repulsion until they reach values of $R < 1$ a.u. The difference between potential curves at $\theta=30°$ and 90° is also explained by the same argument as before. The potential curve at $\theta=60°$ shows a shape more nearly like that at $\theta=0$. This characteristic feature may be understood by the fact that the combination of the strong nuclear repulsion between colliding particles and the nonuniform electron charge distribution of the H_3^+ system with respect to the angle θ is responsible. (We found the oscillatory structure when the adiabatic energy was plotted with fixed R against the θ from 0—90°, continuously.) Alternatively, this may be an artifact due to breakdown of the DIM method at small R. For the $H+H_2^+$ channel, no marked orientation effect of the molecule is observed even for $R < 2$ a.u. This is due to the fact that the H_2^+ ion is less polarized by the presence of the neutral H atom than by the presence of some ions. This results in the flat portion of the $[H + H_2^+(1s\sigma_g)]$ potential curve falling at the $R \gtrsim 3$ a.u. region. The colliding partners do not experience the strong interaction until they reach the region inside $R \sim 3$ a.u.

The same adiabatic potential curves are plotted on Fig. 3. This time, θ is fixed at 30°, while ϕ varies. The differences in shapes of the potentials, corresponding to different values of ϕ are relatively small compared to the θ dependence shown in Fig. 2. We will return to this point in Sec. IV B.

A constant energy gap between the initial- and the charge-transfer channels for values of $R \geq 3.5$ may introduce the Demkov coupling effect. Figure 4 displays the radial coupling between the initial and the charge-transfer states for different molecular orientations. Although the coupling matrix elements exhibit different shapes and magnitudes for $R \leq 4$ a.u., they become identical for $R > 4.5$ a.u. This tail portion of the coupling gives rise to the Demkov coupling effect. Since radial coupling is more sensitive to the nature of the electronic wave function, the deviation in shape among the couplings in the inner region is more remarkable, as expected, compared to that of the potential curves in the same R region.

We have performed two-state close-coupling calculations, involving the initial $H^+ + H_2(X^1\Sigma_g, v=0)$ state and the final $H(1s)+H_2^+(1s\sigma_g, v')$ state. The state corre-

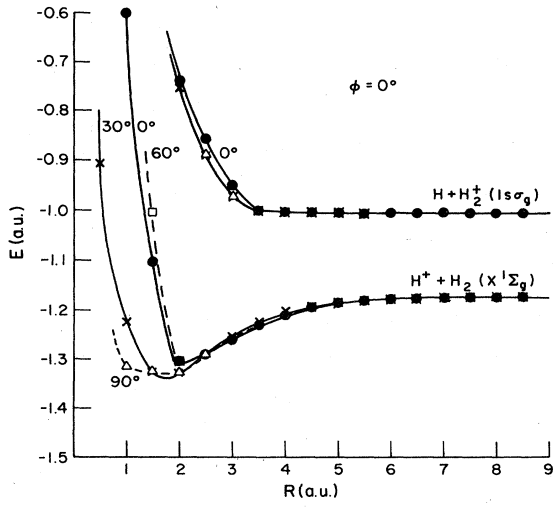

FIG. 2. Adiabatic potential curves as a function of internuclear distance R and angle θ with fixed $\phi=0°$.

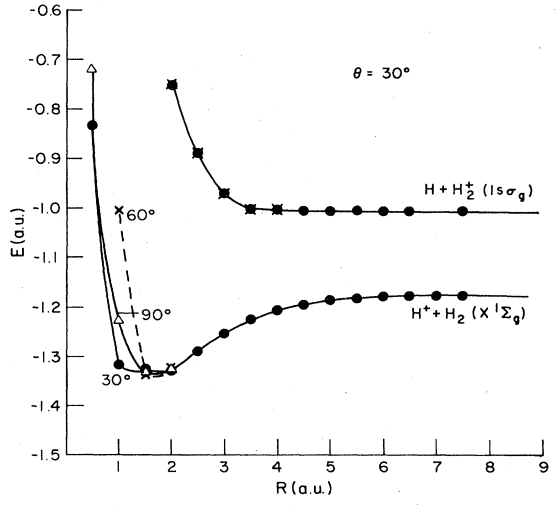

FIG. 3. The same as Fig. 2 but change angle ϕ with fixed $\theta=30°$.

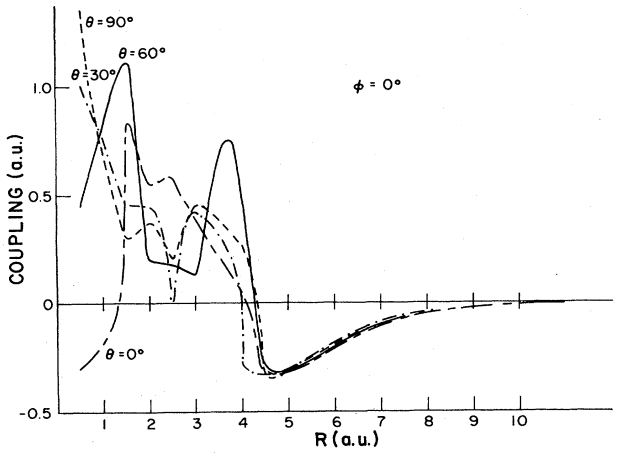

FIG. 4. Radial coupling between $H^+ + H_2(X^1\Sigma_g)$ and $H(1s) + H_2^+(1s\sigma_g)$ states as a function of internuclear distance R and angle θ with fixed ϕ.

sponding to $H(1s) + H_2^+(2p\sigma_u, v')$ has been excluded from the present close-coupling calculation, since the energy gap between the initial and this state is large, and correspondingly, the radial coupling is weak. In addition, the Franck-Condon factor that connects this state with the initial state is much smaller compared to that of the initial $[H^+ + H_2(X^1\Sigma_g)]$ and the first charge-transfer state $[H + H_2^+(1s\sigma_g)]$.

The time evolution of the charge-transfer probability in the two-state close-coupling approximation at $E = 0.6$ keV, $b = 0.5$, is shown in Fig. 5. For the conditions specified by E, b, θ, and ϕ, two or three oscillations of probabilities can be seen during the collision before the electron selects a particular final state. The probability of $\theta = 90°$ has the largest value for these conditions since at this orientation the H_2 molecule provides a favorable close-encounter condition to the projectile. As the angle of the molecular orientation is decreased, the probability becomes smaller. However, this picture holds only for close collisions at this energy. When the conditions are changed, the whole picture is altered.

The impact parameter times the probability has been plotted against the impact parameter at $E = 1$ keV for

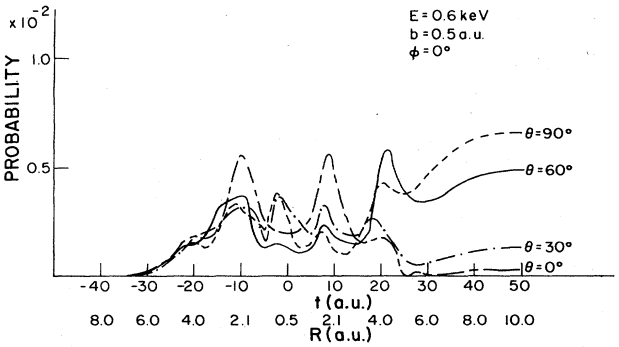

FIG. 5. Time evolution of probabilities at $E = 0.6$ keV, $b = 0.5$ a.u.

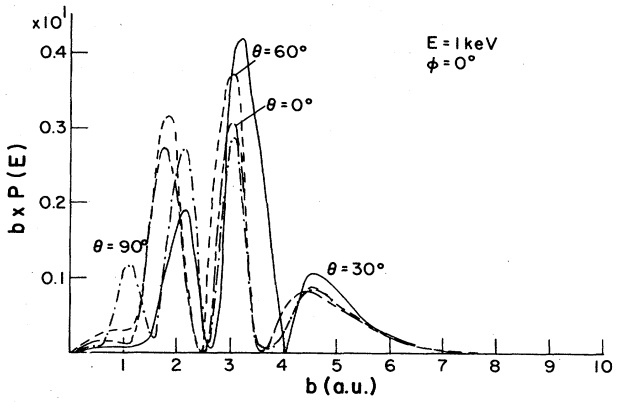

FIG. 6. Probability times impact parameter versus impact parameter as a function of θ at $E = 1$ keV and $\phi = 0°$.

$\phi = 0$ and several choices of θ in Fig. 6. Generally, there are three main peaks corresponding to impact parameters of ~ 2, ~ 3, and 4.5 a.u. for all orientations. Only the $\theta = 90°$ case has a small peak at $b \simeq 1$ a.u., while others show a slight hump or flat at the same impact parameter. In a comparison of the $\theta = 60°$ and 30° cases, $\theta = 30°$ has a larger peak at $b \simeq 3$ a.u. while $\theta = 60°$ has a larger peak at $b \simeq 2$ a.u. The overall area of the probability (cross section) is very similar in these two cases. This trend holds for all orientations This is because of "accidental near-degeneracy" of the probability from different θ. Indeed, calculated cross sections for all orientations are almost identical in the energy range 0.6–6 keV.

The probability times the impact parameter is also plotted against the impact parameter for $\theta = 30°$ and several choices of ϕ in Fig. 7. Again, three main peaks can be seen at $b \sim 2$, 3, and 4.5 a.u., respectively. The remarkable difference between Fig. 7 and Fig. 6 is the fact that the peak at $b \sim 2$ a.u. grows and the peak at 3 a.u. shrinks as the angle ϕ increases. The total area of $P \times b$ (cross section) is quite well balanced by increase and decrease of these peaks and remains nearly constant. Overall, this behavior smears out the molecular orientation effect on ϕ.

To test the energy dependence of the molecular effect, the probability times the impact parameter versus the impact parameter is shown in Figs. 8 and 9, this time, for

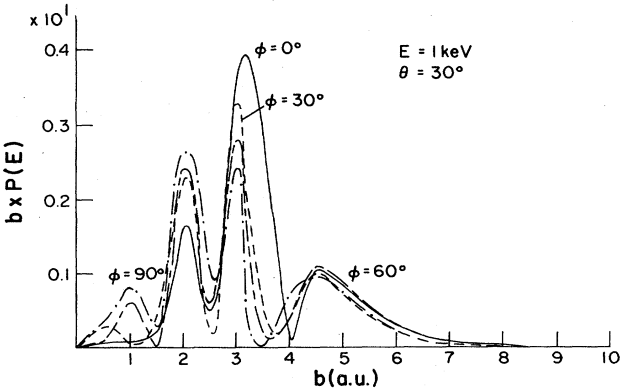

FIG. 7. The same as Fig. 6, but vary ϕ with fixed $\theta = 30°$.

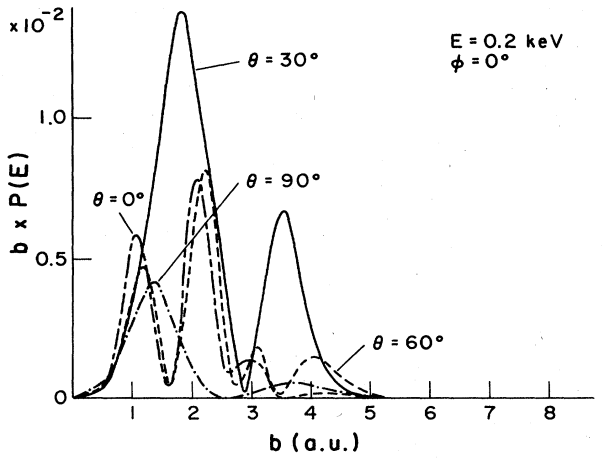

FIG. 8. The same as Fig. 6, except $E=0.2$ keV.

$E=0.2$ and 10 kev with different θ and $\phi=0°$, respectively.

Two main peaks at $b\sim1$ a.u. and ~2 a.u. are observed for $\theta=0°$ and 60°, and one main peak at $b\sim1$ a.u. for the $\theta=90°$ case at $E=0.2$ keV in Fig. 8. Although there are two main peaks in the $\theta=30°$ case, their magnitudes are much larger than others and their locations are at $b\sim1.7$ a.u. and 3.5 a.u., respectively. The orientation effect of the target H_2 molecule at $E=0.2$ keV is much more visible in contrast to the one in Figs. 6 and 7. Another important difference in the feature as seen in Figs. 8 and 6, is that the positions of all peaks are shifted toward smaller b in the lower-energy case shown in Fig. 8. This implies that at this energy, the close collision is the main mechanism for the charge transfer. Again, departure from the "accidental near-degeneracy" in the transition probability can be seen in the higher energy case of $E=10$ keV in Fig. 9. Again, two main peaks are found at $b\sim1$ a.u. and 3.5–4.0 a.u. for all θ. However, the magnitude of each peak is quite different for each θ, and this leads to different values of the cross section for each θ. Although the position of the outer peak is around 3.5

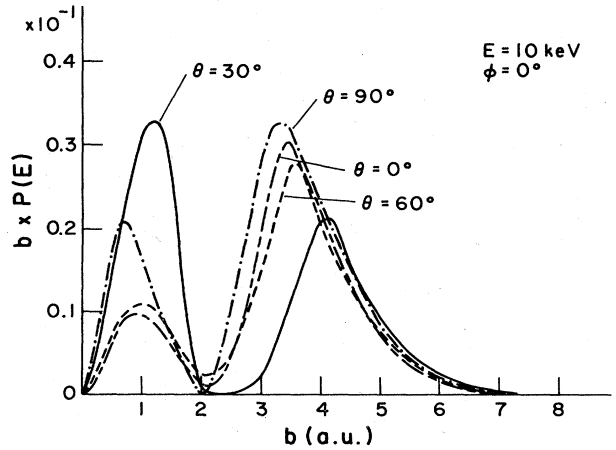

FIG. 9. The same as Fig. 6, except $E=10$ keV.

TABLE II. Charge-transfer cross section for $H^+ + H_2(X^1\Sigma_g, \theta, v=0) \rightarrow H(1s) + H_2^+(1s\sigma_g, v'=4)$ at fixed $\phi=0°$. The digits enclosed in parentheses are powers of 10 by which the numbers are multiplied.

	Cross section (10^{-16} cm^2)			
E (kev)	$\theta=0°$	$\theta=30°$	$\theta=60°$	$\theta=90°$
0.2	1.562(−2)	4.026(−2)	1.720(−2)	0.898(−2)
0.4	1.667(−2)	6.649(−2)	2.631(−2)	3.474(−2)
0.6	6.043(−2)	8.968(−2)	6.829(−2)	4.961(−2)
1.0	8.922(−2)	1.088(−1)	9.917(−2)	9.517(−2)
2.0	1.21(−1)	1.26(−1)	1.23(−1)	1.45(−1)
4.0	1.33(−1)	1.33(−1)	1.30(−1)	1.73(−1)
6.0	1.20(−1)	1.46(−1)	1.17(−1)	1.59(−1)
10.0	1.02(−1)	1.22(−1)	9.901(−2)	1.34(−1)

a.u. as was seen in Figs. 6 and 7, the inner peak located at $b\sim1$ a.u. grows dramatically as the energy increases, but no notable peak is seen in this region in Figs. 6 and 7. This suggests that the close collision mechanism becomes important to the charge-transfer process at the energy above $E\sim10$ keV.

B. Cross sections

Cross sections $\sigma(E,\theta)$ for electron capture into the $H(1s)$ state, leaving the $H_2^+(1s\sigma_g)$ ion in the vibrational state $v'=4$ are given in Table II. Also, the cross section $\sigma(E,\phi)$ for electron capture into the $H(1s)$ state is tabulated in Table III. First, let us discuss the results in Table II. The influence of molecular orientation effects on the cross sections is not apparent for collision energies between 0.6 and 6 keV. Between these energies, the cross section is close regardless of the molecular orientation as is discussed in the previous section as the effect of the accidental near-degeneracy. The difference between the largest and the smallest cross sections in this energy range is less than 30%. Obviously, this characteristic is easily understood, since a distant collision is an important mechanism when the cross section shows its maximum. The collision dynamics between the colliding partners is over before the projectile sees a real molecule. Above or below this energy range, the molecular effect might come clearly into the

TABLE III. Charge-transfer cross section for $H^+ + H_2(X^1\Sigma_g, \phi, v=0) \rightarrow H(1s) + H_2^+(1s\sigma_g, v'=4)$ at fixed $\theta=30°$. The digits enclosed in parentheses are powers of ten by which the numbers are multiplied.

	Cross section (10^{-16} cm^2)		
E (keV)	$\phi=30°$	$\phi=60°$	$\phi=90°$
0.2	9.989(−2)	7.646(−3)	8.373(−3)
0.4	3.540(−2)	4.162(−2)	3.696(−2)
0.6	6.42(−2)	5.733(−2)	5.485(−2)
1.0	8.820(−2)	9.139(−2)	9.551(−2)
2.0	1.479(−1)	1.479(−1)	1.334(−1)
4.0	1.124(−1)	1.870(−1)	1.443(−1)
6.0	1.087(−1)	1.884(−1)	1.450(−1)
10.0	9.206(−2)	1.450(−1)	1.242(−1)

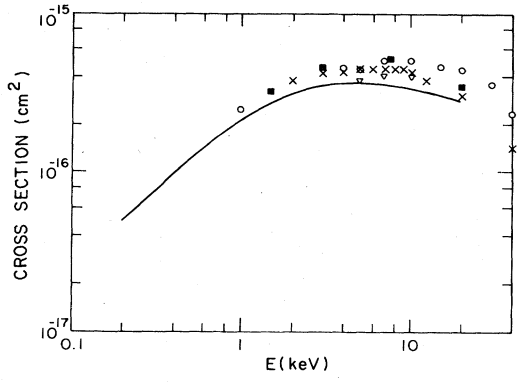

FIG. 10. Charge-transfer cross section on the process $H^+ + H_2(X^1\Sigma_g) \rightarrow H(1s) + H_2^+(1s\sigma_g)$ as a function of incident energy. Theory: solid line. Experiment: ○, Ref. 23; ■, Ref. 22; ×, Ref. 21; ▽, Ref. 24.

cross section because a close collision becomes an important mechanism (see also Figs. 8 and 9). In fact, we can notice a gradual increase of the molecular effect in the cross section below 0.6 keV. At 0.2 keV, the lowest energy we studied, the cross section at $\theta = 30°$ makes the most dominant contribution to the total cross section and, actually, this cross section is about four times larger than the cross section at $\theta = 90°$ which is the smallest of all. Above 6 keV, again, the molecular effect becomes apparent. The ratio between the largest cross section at $\theta = 90°$ and the smallest at $\theta = 0°$ is more than 50%. This should increase as the collision energy increases.

Turning to Table III, which represents the cross section at fixed $\theta(=30°)$ and varying $\phi(=30°, 60°, 90°)$, we notice that the orientation effect on $\phi(\geq 30°)$ is less pronounced. At 1 keV, the difference between the largest and the smallest cross section is less than 8%. Although this number increases up to 24% at 0.2 keV, it might be concluded safely that the molecular effect of rotating the molecule with ϕ is considerably smaller or actually washed out (see also Fig. 7). This is again due to the accidental near-degeneracy of the cross section of each ϕ.

Total cross section $\sigma(E)$, after integrating with respect to the orientation angle θ and ϕ (calculated step size is 2° for both θ and ϕ), and summing all the vibrational states of the $H_2^+(1s\sigma_g)$ molecular ion ($v' = 0-10$), is plotted in Fig. 10 along with experimental measurements.[21–24] Our results are qualitatively in good accord with all experimental data in the energy range where they are available.

Our results are about 20% lower compared to the data of Williams and Dunbar.[21] (They claim that their experimental error is within 5%.) At the higher energy ($E > 10$ keV), our result may tend to overestimate the cross section. Indeed, the shape of our cross section above 10 keV looks flatter than that of the measurements. The charge transfer to the excited states of the hydrogen atom as well as the excitation of the H_2 molecule becomes important in this energy region, which is not accounted for in the present work. Below 0.2 keV, our method may not offer accurate cross sections in view of our neglect of other inelastic channels like the vibrational excitation and the rearrangement channels, which are considered to be dominant processes. Judging the approximate method employed in this work, the agreement between the present result and the measurement is considered to be satisfactory.

At least for high-energy impact, it was assumed that the charge-transfer cross section in the $H^+ + H_2$ collision is one-half that for the $H^+ + H$ collision, since the target H_2 molecule behaves like two independent H atoms. The validity of this assumption was tested by Tuan and Gerjuoy,[11] who concluded that although their calculated result is fortuitously in good accord with the assumption for the collision energy up to 400 keV, this is largely due to accidental cancellation of different effects. Their ratio of total-charge-transfer cross section for $H^+ + H$ and $H^+ + H_2$ processes as a function of energy is almost constant with the value ~0.5 in the energy range below 120 keV in remarkable contrast to the one obtained by Band,[12] in which the ratio is about 0.55 at 25 keV and decreases to ~0.35 at 125 keV. Our calculated result for this ratio is shown in Table IV. Although the qualitative shape of our ratio below 20 keV seems to be in good accord with the one obtained by Band[12] using the perturbation method, the discrepancy of the magnitude of the ratio at $E = 20$ keV is approximately a factor of 3. Compared to the charge-transfer process in the $H^+ + H$ collision which is an exact resonant charge-transfer process, the one in the $H^+ + H_2$ collision is a nonresonant process with an energy defect of 0.105 a.u. The charge-transfer cross section of this system shows a maximum around 4 keV and drops off rapidly on both sides of the energy as is typically the case for the nonresonant charge-transfer process. This leads to the much smaller cross section in the $H^+ + H_2$ collision in comparison to that of the symmetric resonant $H^+ + H$ collision at the lower energy, say, $E \leq 4$ eV. As the energy increases, colliding particles have enough energy to surmount the energy defect between initial and final states and therefore, the ratio of the cross section decreases within the energy range studied. In this energy range of the present work, the molecular nature of the target H_2 molecule persists as we have seen above and correspondingly the assumption that a diatomic molecule behaves like independent constituent atoms has completely failed. In the higher-energy region $E \geq 25$ keV, the result of Band[12] seems to approach a certain constant value asymptotically. Although two asymptotic values reported by Tuan and Gerjuoy[11] and by Band[12] differ markedly, apparently they showed that such an assumption could be incorrect.

TABLE IV. Ratio $\sigma(H)^a/\sigma(H_2)$.[b] $\sigma(H)$: $H^+ + H(1s) \rightarrow H(1s) + H^+$. $\sigma(H_2)$: $H^+ + H_2(X^1\Sigma_g) \rightarrow H(1s) + H_2^+(1s\sigma_g)$.

	Cross section (cm²)		
E (keV)	σ (H)	σ (H_2)	$\sigma(H)/\sigma(H_2)$
1.0	1.42^{-15}	2.11^{-16}	6.73
2.0	1.37	3.13	4.38
4.0	1.18	3.67	3.22
6.0	0.998	3.62	2.76
10.0	0.741	3.41	2.17
20.0	0.621	2.85	2.18

[a]Reference 25.
[b]This work.

V. CONCLUSION

The molecular-orbital—expansion method incorporating the ETF effect has been applied to investigate the charge transfer in $H^+ + H_2(X^1\Sigma_g, v=0)$ collisions in the energy range from 0.2 to 20 keV. The result shows that although, due to the accidental near-degeneracy of the charge-transfer probability from the different θ, the orientation effect of the target H_2 molecule on the charge-transfer mechanism is not so notable in the energy region where the cross section has its maximum, this is marked in the energy range below 0.5 keV and above 10 keV since close collisions become important mechanisms in these energy regions. Evidently, this fact indicates that treating the target H_2 molecule as a sum of two independent H atoms in the study of the charge transfer is incorrect in the energy range studied.

ACKNOWLEDGMENTS

The author would like to thank Dr. N. F. Lane for useful discussions. This work was supported by the U.S. Department of Energy (Office of Basic Energy Sciences).

[1]M. Kimura and W. R. Thorson, Phys. Rev. A **24**, 1780 (1981).
[2]M. Kimura and W. R. Thorson, Phys. Rev. A **24**, 3019 (1981).
[3]M. Kimura, R. E. Olson, and J. Pascale, Phys. Rev. A **26**, 3113 (1982).
[4]T. G. Winter and G. J. Hatton, Phys. Rev. A **21**, 793 (1980).
[5]T. G. Winter, G. J. Hatton, and N. F. Lane, Phys. Rev. A **22**, 930 (1980).
[6]W. Fritsch and C. D. Lin, Phys. Rev. A **26**, 762 (1982).
[7]T. G. Winter and C. D. Lin, Phys. Rev. A **29**, 567 (1984).
[8]W. Fritsch and C. D. Lin, Phys. Rev. A **29**, 3039 (1984).
[9]D. P. Sural and N. C. Sil, J. Chem. Phys. **42**, 729 (1965).
[10]V. Sidis and D. de Bruijn, Chem. Phys. **85**, 201 (1984).
[11]T. F. Tuan and E. Gerjuoy, Phys. Rev. **117**, 756 (1960).
[12]Y. B. Band, J. Phys. B **15**, 2055 (1974).
[13]F. O. Ellison, J. Am. Chem. Soc. **85**, 3540 (1963); **85**, 3544 (1963); **86**, 2115 (1984).
[14](a) J. C. Tully, J. Chem. Phys. **58**, 1396 (1973); (b) **59**, 5122 (1973).
[15]R. K. Preston and J. C. Tully, J. Chem. Phys. **54**, 4297 (1971); J. C. Tully and R. K. Preston, *ibid.* **55**, 562 (1971).
[16]P. J. Kuntz and A. C. Roach, J. Chem. Soc. Faraday Trans. II **68**, 259 (1972).
[17]W. Kolos and L. Wolniewicz, J. Chem. Phys. **43**, 2429 (1965).
[18]D. R. Bates and T. R. Carson, Proc. R. Soc. London, Ser. A **234**, 207 (1956).
[19]J. B. Delos, Rev. Mod. Phys. **53**, 287 (1981).
[20]H. Conroy, J. Chem. Phys. **51**, 3979 (1969).
[21]J. F. Williams and D. N. Dunbar, Phys. Rev. **149**, 62 (1966).
[22]O. Hollricher, Z. Phys. **187**, 41 (1965).
[23]Yu. S. Gordeev and M. N. Panov, Sov. Phys.—JETP **9**, 656 (1964).
[24]F. J. de Heer, J. Schutten, and H. Moustafa, Physica (Utrecht) **32**, 1768 (1966).
[25]For a 10-MO close-coupling calculation see M. Kimura (unpublished).